Int J Adv Manuf Technol (2011) 56:1039–1048
DOI 10.1007/s00170-011-3247-0

ORIGINAL ARTICLE

Finite element analysis on neck-spinning process of tube at elevated temperature

Chi-Chen Huang · Jung-Chung Hung · Chinghua Hung · Chia-Rung Lin

Received: 28 September 2010 / Accepted: 27 February 2011 / Published online: 11 March 2011

Abstract Tube spinning process is a metal forming process used in the manufacture of axisymmetric products and has been widely used in various applications. Finite element analysis has been successfully applied to the tube spinning processes, but no temperature effects have been considered on neck-spinning. For this reason, the aim of this research is to investigate numerically the neck-spinning process of a tube at elevated temperature. The commercial software Abaqus/Explicit was adopted in the simulation. For the construction of the material model, special uniaxial tensile tests were conducted at elevated temperature and various strain rates, since the material is sensitive to strain rates at high temperature. Comparisons between experimental and simulation results on thickness distribution and the outer contour of the spun tube are discussed. During the final stage, the average deviations between the simulation and experiment were 10.65% in thickness and 3.03% in outer contour. Good agreement was found between experimental and simulation results. The influence of the coefficient of friction, roller translation speeds, and the tip radius of the rollers were also investigated through numerical simulation.

C.-C. Huang · C. Hung (✉)
Department of Mechanical Engineering,
National Chiao Tung University,
1001 University Road, Hsinchu 30010 Taiwan, Republic of China
e-mail: chhung@mail.nctu.edu.tw

J.-C. Hung
Department of Mechanical Engineering,
National Chin-Yi University of Technology,
Taiping, Taichung, Taiwan, Republic of China

C.-R. Lin
Mosa Industrial Corporation,
Huwei, Yunlin, Taiwan, Republic of China

Keywords Finite element analysis · Hot neck-spinning · Strain rate · Tube spinning

1 Introduction

The tube spinning process is a metal forming process used in the manufacture of axisymmetric products. The process is often used to manufacture high-precision and high-strength tubular components. The spinning process makes it easy to control the dimensions of the tube. The strength of the tube also increases during the process. Other advantages include a high material usage rate, fewer processing stages, a low forming force, die-less, and flexibility in manufacturing. For these reasons, tube spinning process has been widely used in various applications.

Several researchers have conducted experimental and theoretical investigations on the influence of the various parameters on the spinning process [1–8]. Progress in computation capability and software coding has enabled the application of finite element (FE) analysis to the tube spinning process. Hauk et al. [9] used an axisymmetric model and a 1/36 three-dimensional (3D) model to simulate the flow-splitting process. They compared the difference between results of 2D and 3D models. Iguchi et al. [10] used a dynamic explicit code DYNA-3D to analyze the spinning manufacturing process for exhaust system components of motor vehicles. The results showed the distribution of stress and strain which evolved in the material during spinning. This provided useful information for the prediction of failures during spinning. Hua et al. [11] used ANSYS to establish a 3D elastic–plastic finite model for the three-roller backward spinning of a cylindrical workpiece. The simulation results showed a variety of phenomena that occur during spinning. These included bell-mouth

distortion, build-up, bulging in the front of and between the rollers, and diametral reduction and growth. Xia et al. [12] used MARC to simulate the process of multipass offset tube neck-spinning. Their results showed that the distribution of strain and stress is nonaxisymmetric; the equivalent stress distributes and varies along the axial direction section by section and reaches a maximum at the opening end of the spun workpiece. The thickness reduction at the opening end, and the ellipticity and axial elongation of the spun workpiece increased with increasing spinning passes. The linearity of forward path spinning was significantly less than that of backward path spinning. Parsa et al. [13] used an explicit commercial finite element program to simulate forward flow forming of tubes. The effects of attack angles and feed rates on the flow formability have been evaluated. Li et al. [14] used finite element software MSC.Marc to simulate the cross-section forming of axially inner grooved copper tube. The results show that gaps in the groove walls are caused not only by the diametric clearance between the inner wall of the copper tube and the mandrel but also by the bending deformation of the copper tube.

In the above literature, the tube spinning processes were all performed at room temperature. Figure 1 shows that performing the spinning process at room temperature will cause a fracture to occur at the top of the tubes, especially when deformation is large. However, few studies have mentioned tube spinning at elevated temperature. Makoto et al. [15] invented a new computer numerical control (CNC) spinning machine comprised of rollers with heaters. The heated rollers heated the magnesium tubes and formed them into various shapes by spinning. The forming possibility of magnesium tubes was experimentally demonstrated. Mori et al. [16] developed a hot shear spinning process of cast aluminum ally parts to eliminate casting defects and obtain a desired distribution of wall thickness. Hot air heated the blank during the shear spinning process to maintain the forming temperature at 400°C. Yang et al. [17] established a 3D coupled thermomechanical FE model of the hot splitting spinning process of magnesium alloy AZ31. The influence of different initial temperatures of the disk blank and different feed rates of the splitting rollers on forming quality of deformed flanges was investigated numerically.

In summary, finite element analysis has been successfully applied to the tube spinning processes, but no temperature effects have been considered on neck-spinning. For this reason, the aim of this research was to investigate numerically the neck-spinning process of tubes at elevated temperature. Comparing the results of the simulation and the experiment would verify the finite element model. The influence of the process parameters is also discussed.

2 Experiment

Figure 2 is a photograph of a spinning machine. There are two rollers in the machine, which are controlled by CNC. The tubes adopted in this work were made from a JIS G3141 steel sheet using deep drawing processes. Figure 3 shows the dimensions of the tube and roller.

The procedure of neck-spinning at an elevated temperature included three steps. First, the tube was heated to the forming temperature (1,000°C) by a high frequency induction heater. The tube was then formed by rollers without heating in the second step. Table 1 lists the forming conditions. The tube was clamped on the spindle and rotated at 1,800 rpm, and the rollers translation speed was 20 mm/s. The four spinning stages were performed sequentially and the roller paths are shown as Fig. 4. In Fig. 4, the solid lines represent the forming paths and the dashed lines represent the rapid linear movement between the end of the stage and the next stage. The total time of the

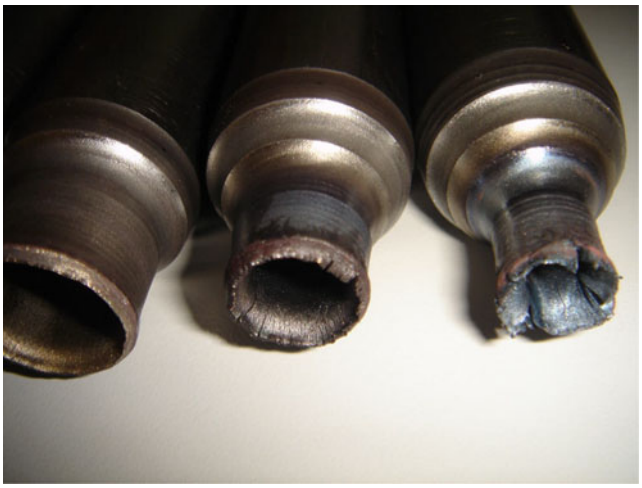

Fig. 1 Fracture after spinning at room temperature

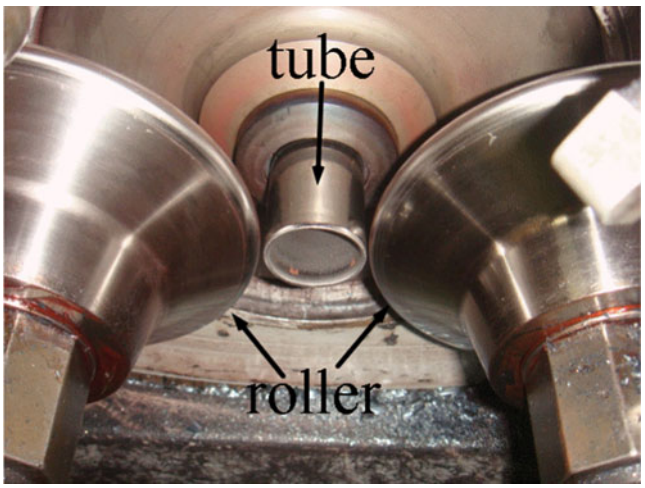

Fig. 2 Photo of spinning machine

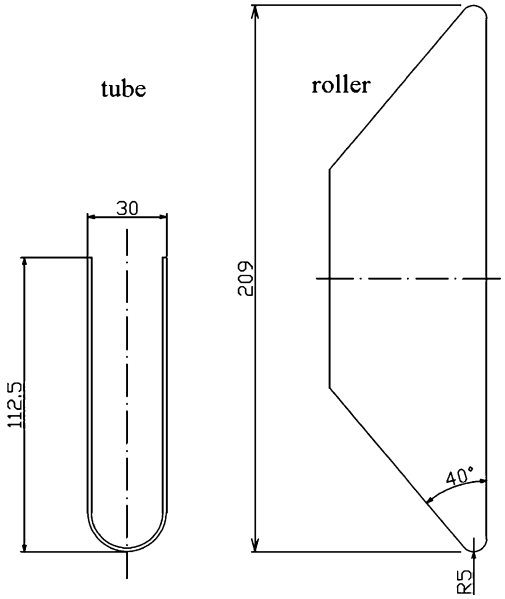

Fig. 3 Dimensions of tube and roller

four-stage spinning process was 5.628 s. After forming, the tube was quickly cooled to room temperature using compressed air. Figure 5 shows the results of neck-spinning on the tubes after each of the four stages.

3 Finite element analysis

In this study, the commercial software Abaqus/Explicit was used to simulate the neck-spinning of a tube at an elevated temperature. The following assumptions were adopted to establish the FEA model:

1. The tube is isotropic and homogenous with an elastic–plastic response,
2. The rollers are treated as rigid bodies, and
3. The tube is isothermal during each spinning stage.

Figure 6 shows the FEA model. Only a partial tube was constructed in the model because the bottom part of the tube (70 mm from the bottom) was fixed by a clamp during the experiment. All degrees of freedom were fixed at the bottom nodes of the model in the simulation. The tube was discretized by four-node shell elements with full integration. The element size was 1×1.5 mm in the large deformation zone and 1.5×1.5 mm in the remaining part of the model; 2,340 nodes and 2,280 elements were in the

Table 1 Forming condition

Forming temperature (°C)	1,000
Rotational speed of the spindle (rpm)	1,800
Roller translation speed (mm/s)	20

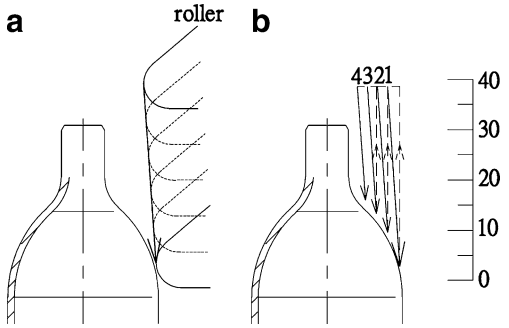

Fig. 4 Schematic of roller moving path. **a** First stage. **b** Four stages

FEA model. The tube was made by deep drawing process so that the thickness distribution on the tube was not uniform. The initial thickness distribution of tube in simulation (Fig. 7) was measured from the actual tube.

In the actual forming process, the tube rotates around its axis and the rollers rotate freely while making contact with it. However, a large number of rotations of a deformable body may result in a volume change and numerical error in FE analysis [10, 18]. Therefore, in this study, the tube was fixed and the rollers revolved around the axis of the tube. The revolving speed was equal to the rotational speed of the spindle in experiment. In a hot working process, the typical coefficient of friction was found experimentally to be 0.4 [19]. Thus, the coefficient of friction in the interface between the tube and rollers was assumed as 0.4. The initial temperature of the tube was 1,000°C in the simulation, and the tube was isothermal during each spinning stage.

At high temperatures, the material properties are sensitive to strain rates. In this case, the strain rate value was as high as $30s^{-1}$ during the hot spinning process. Therefore, the simulation should include the strain rate effect of flow stress. Special uniaxial tensile tests were executed at elevated temperature and various strain rates using DSI

Fig. 5 Four stages of spun tubes

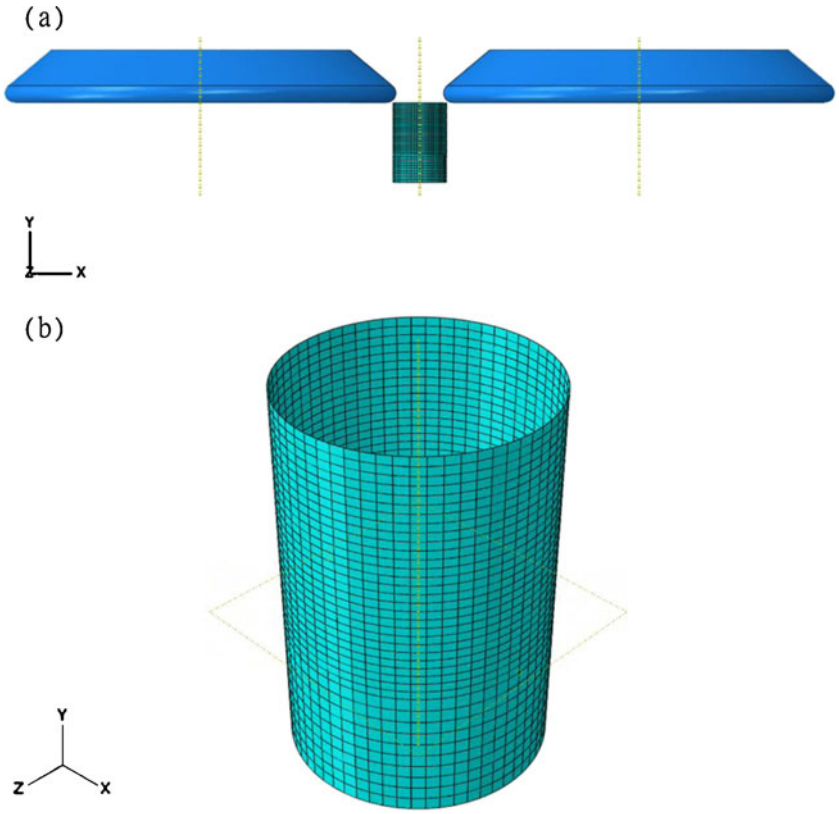

Fig. 6 FEA model: **a** whole model, **b** tube

Gleeble3500, which is designed for dynamic thermal–mechanical material testing. Figure 8 shows the results of the tensile tests at 1,000°C. As the strain rate increased, the signal noise became larger. A uniaxial tensile test was also executed at $\dot{\varepsilon} = 10s^{-1}$, but the noise and signal were difficult to identify. A power law form was used to fit the three stress–strain curves, and the fitted results were input into the simulation. To reduce the computational time, the mass scaling factor was chosen as 50 and the process was sped up two times during the simulation. The total time of the four-stage spinning process was 1.705362 s in the simulation, and the initial time increment was 1.135×10^{-6} s. The number of increments was quite large during the simulation so a double precision option was used to avoid the effect of round-off errors. With the current chosen mass scaling factor and time scaling factor, the simulation was completed in 15 h and 42 min by a personal computer.

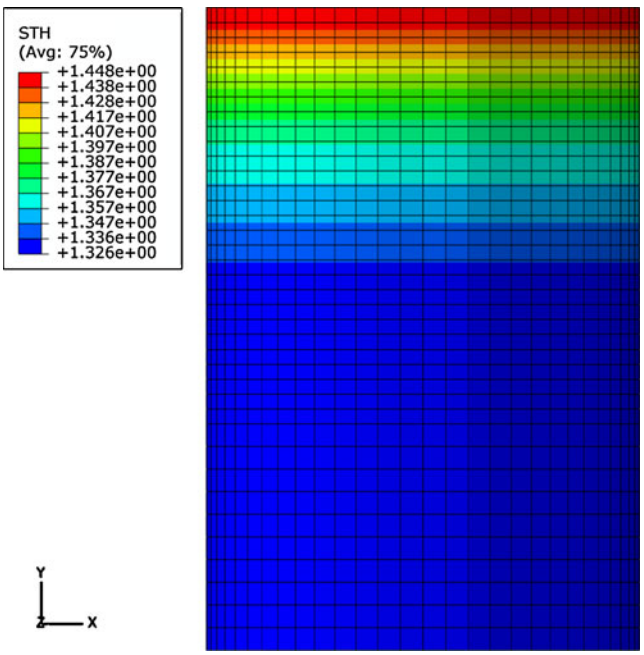

Fig. 7 Initial thickness distribution of tube in the simulation

4 Result and discussion

4.1 Verification of finite element model

To make sure that the result of the explicit solver is close to a quasi-static solution, the kinetic energy of the deforming material should not exceed a small fraction (typically 5% to 10%) of the internal energy throughout most of the simulation (Getting Started with Abaqus, Dassault Systemes). Figure 9 shows the ratio of the kinetic energy (ALLKE) to the internal energy (ALLIE), which was below 2% for the entire simulation time. Therefore, the use of mass scaling factor and the speed up of process tour are reasonable.

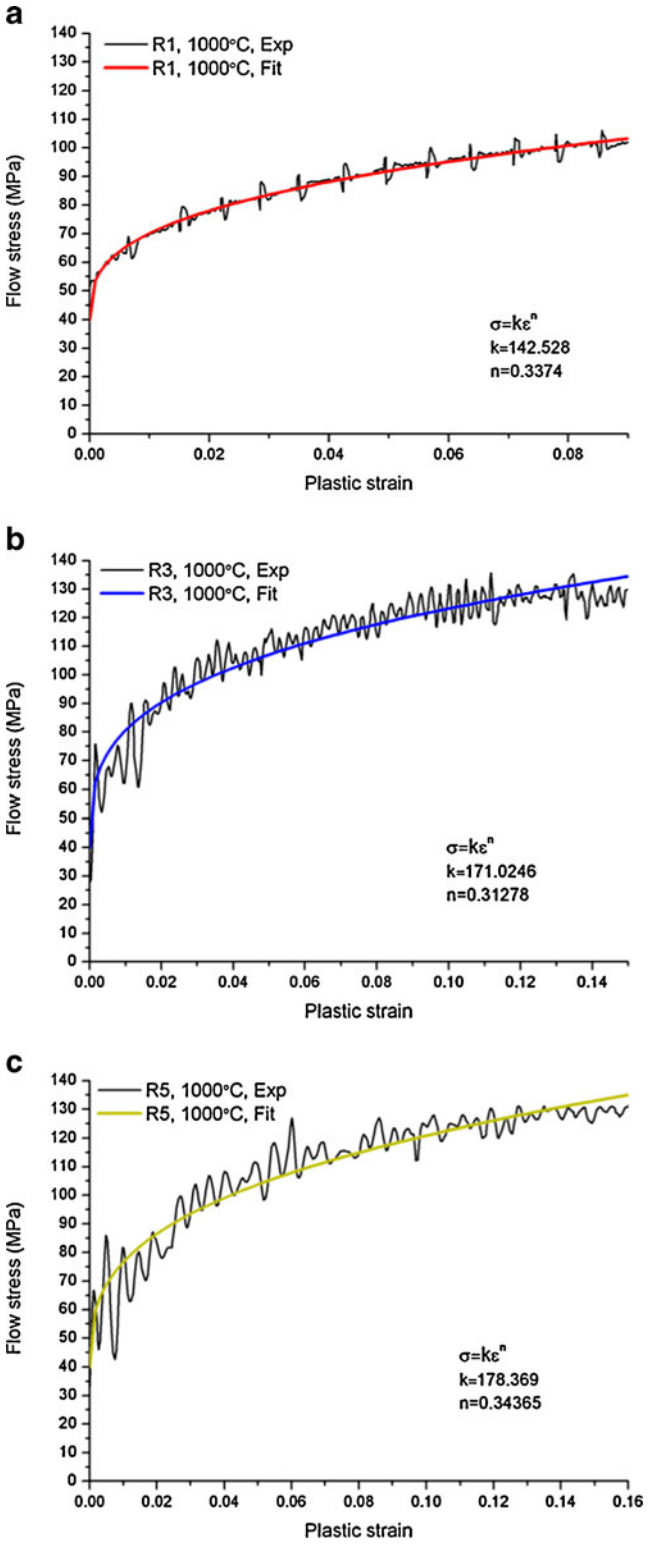

Fig. 8 Stress–strain curves at 1,000°C and various strain rates: **a** $\dot{\varepsilon} = 1s^{-1}$, **b** $\dot{\varepsilon} = 3s^{-1}$, **c** $\dot{\varepsilon} = 5s^{-1}$

Figure 10 shows the simulation results of equivalent plastic strain after each spinning stage. The maximum value of the equivalent plastic strain was approximately 10 at the top of the tube. This equivalent plastic strain is quite large, so it would be difficult to produce this tube at room temperature in so few stages. At the top of the tube, a bell-mouth occurred at each stage. This same phenomenon occurred in the experiment (Fig. 5).

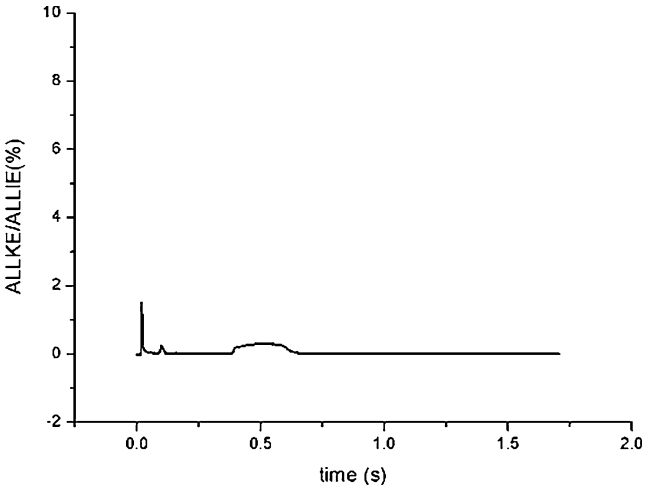

Fig. 9 Ratio of the kinetic energy to the internal energy

Figure 11 shows the comparison of thickness distribution between the simulation and experimental results after each stage. In both simulation and experiment, the thickness increased as the spinning process increased. From the first to the fourth stage, the average deviations between the simulation and experiment for the thickness were 3.51%, 5.15%, 8.4%, and 10.65%, respectively. During the first two stages, the simulation results of thickness corresponded well with those of the experiment. The deviation of thickness between the simulation and the experiment increased slightly during the final stage, but the tendency is consistent. Two factors may cause a deviation of thickness. First, the temperature field was assumed to be isothermal in the simulation, but in reality, the temperature may change during the process. Temperature change will probably have some affect on material properties. Second, after three stages, the quality of the mesh was poor in the upper tube region. Poor mesh quality may result in further numerical errors.

Figure 12 shows the comparison of the outer contour of the tube in the simulation and the experiment after each stage. From the first to the fourth stage, the average deviations between the simulation and experiment for the outer contour were 1.05%, 1.43%, 1.9%, and 3.03%, respectively. The simulation results are in agreement with the experimental results. Figure 13 shows a full-scale figure of the simulated and experimental tube. The simulated tube is a slightly narrower than the experimental tube.

Although there is a slight deviation in thickness between simulation and experimental results at the final stage, the FE model of neck-spinning of tube at elevated temperature

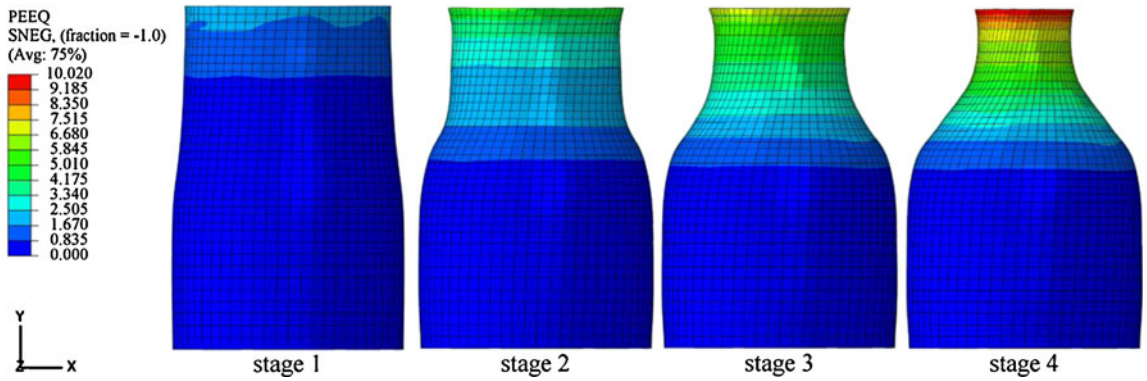

Fig. 10 Equivalent plastic strain of each stage

is still reliable. The FE model can be used to find the proper parameters for the neck-spinning process. This usage is more efficient than experiments dependent on trial and error.

4.2 The influences of coefficient of friction

In the above simulation, the coefficient of friction in the interface between the tube and rollers was assumed as 0.4. This coefficient is typical for hot working; however, this actual contact property is difficult to measure in tube spinning at elevated temperatures. Therefore, various coefficients of friction (0.1, 0.2, 0.3, 0.4, and 0.5) were used in the simulations. Three indexes are used to discuss the results. They are (1) the radius deviation, (2) ellipticity, and (3) the twisting angle. The radius deviation is defined as the standard deviation of the outer radius at the same cross section of the tube. The ellipticity is defined as the difference between the maximum and minimum radius at the same cross section of the tube [12]. The radius deviation

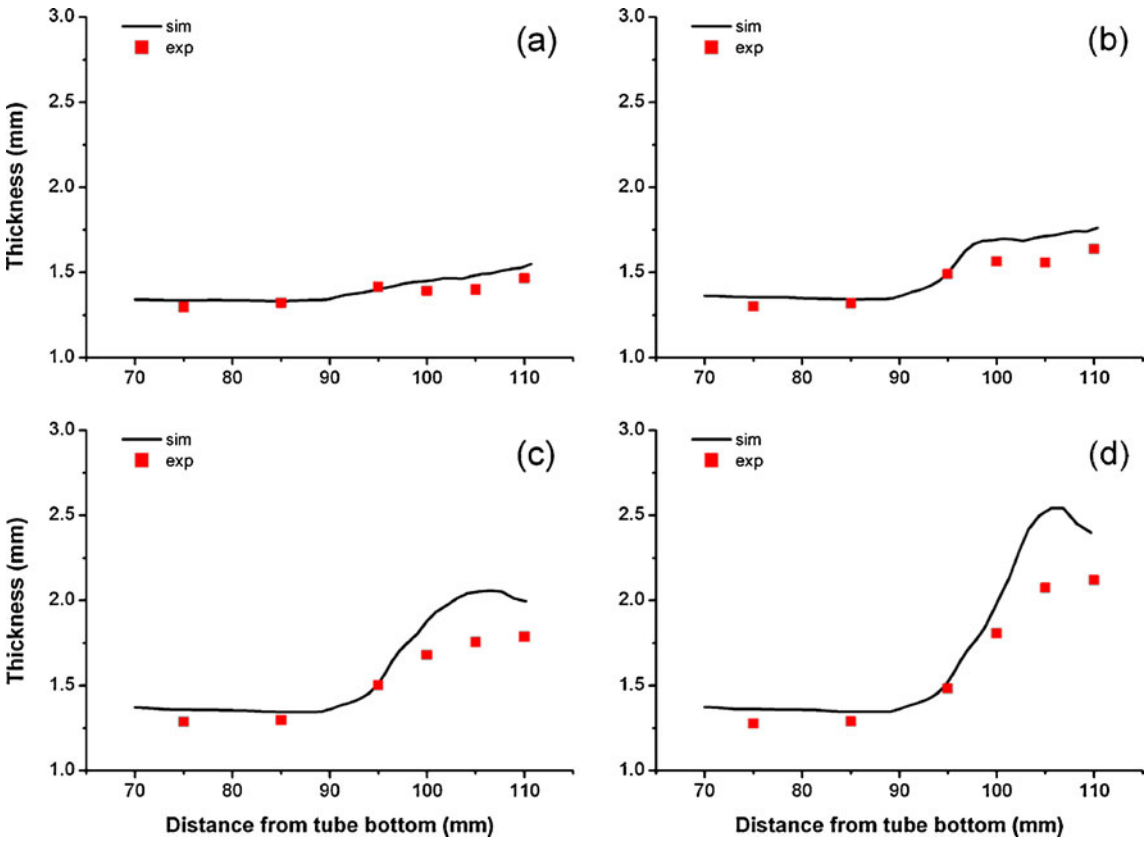

Fig. 11 Comparison between experimental and simulation results for the thickness: **a** stage 1, **b** stage 2, **c** stage3, **d** stage4

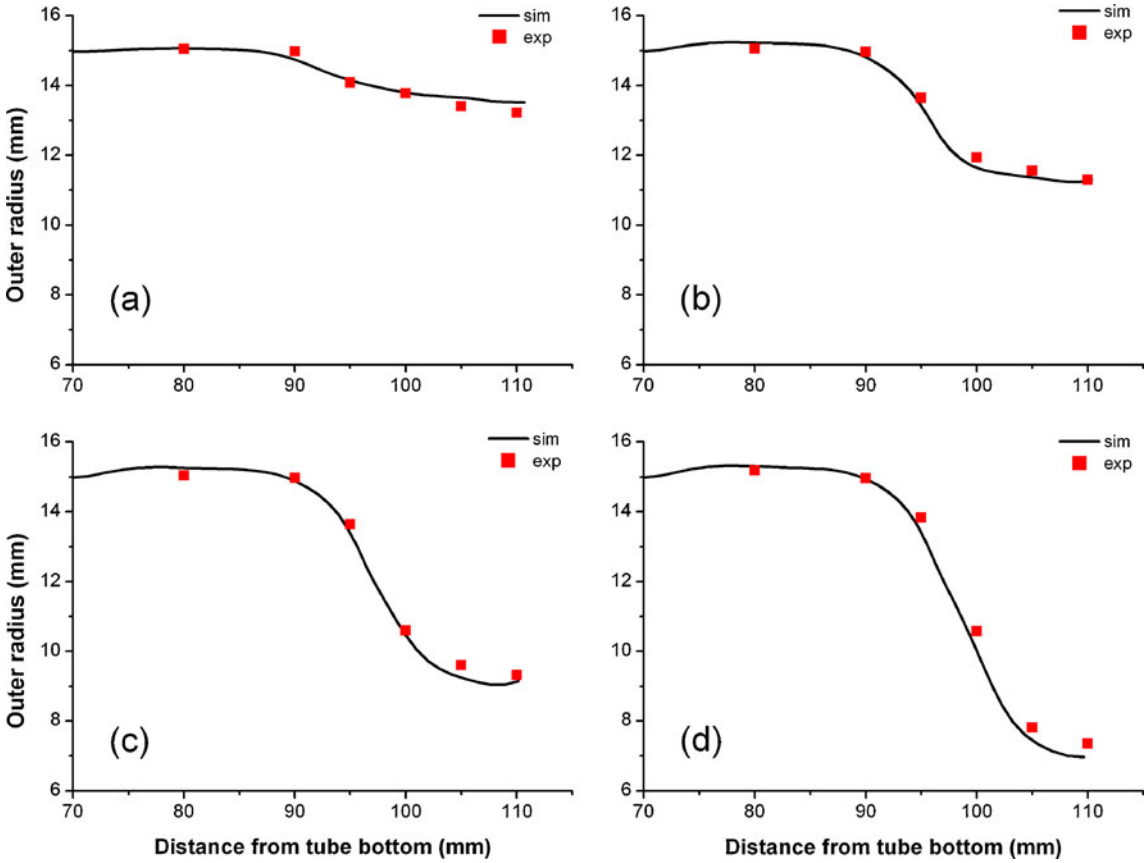

Fig. 12 Comparison between experimental and simulation results for the outer contour of the tube: **a** stage 1, **b** stage 2, **c** stage 3, **d** stage 4

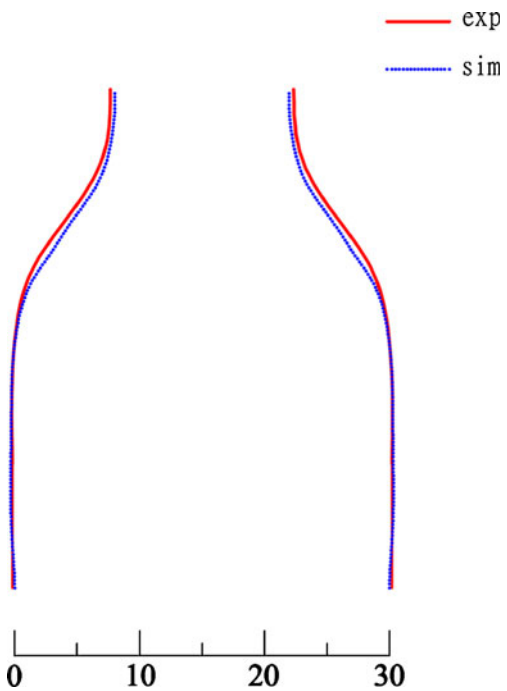

Fig. 13 Comparison between experimental and simulation results of outer contour at the fourth stage (unit: millimeters)

and ellipticity are similar in that they indicate the roundness of the tube. The twisting angle is defined as the twisting angle between the top and bottom of the tube.

Figure 14 shows the influence of the coefficient of friction on roundness. When the coefficient of friction was larger than 0.2, the radius deviation and ellipticity decreased as the coefficient of friction increased. Figure 15 shows the influence of the coefficient of friction on the twisting angle. The twisting angle increased significantly as

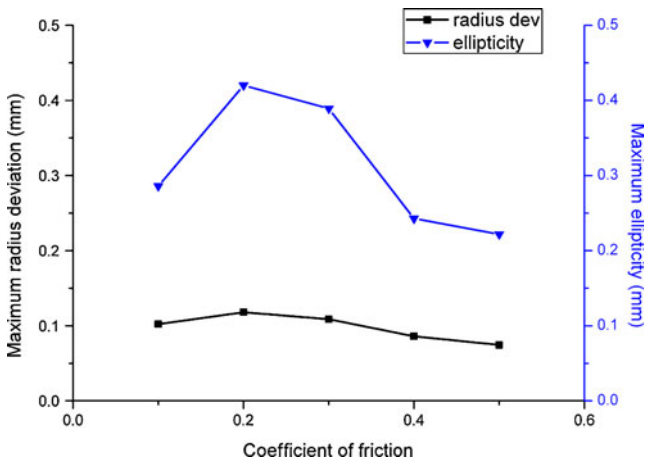

Fig. 14 The influence of the coefficient of friction on roundness

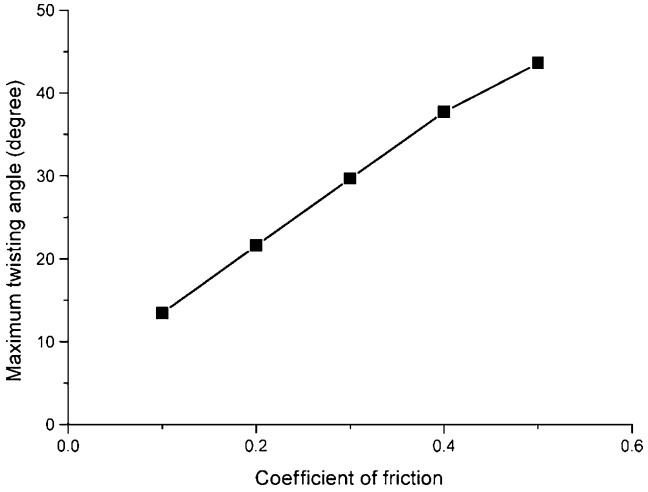

Fig. 15 The influence of the coefficient of friction on the twisting angle

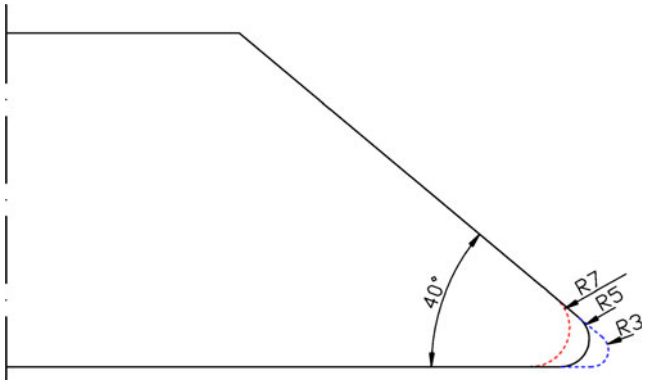

Fig. 18 Dimension of roller with various tip radiuses

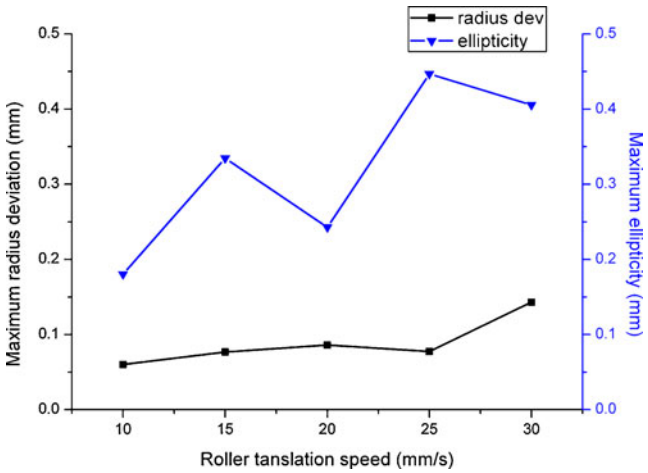

Fig. 16 The influence of roller translation speed on roundness

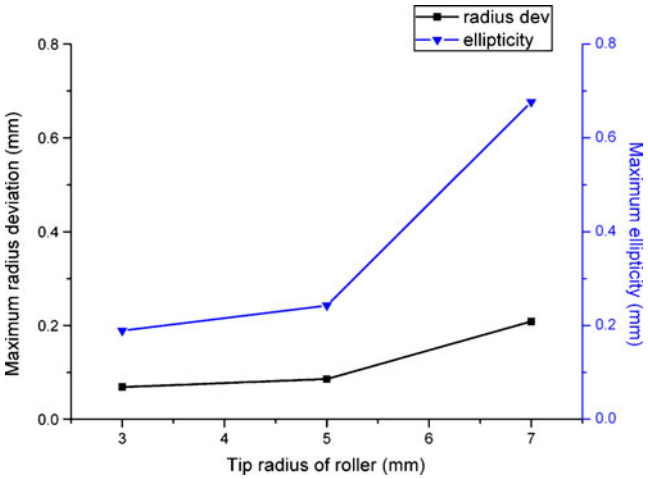

Fig. 19 The influence of roller tip radius on roundness

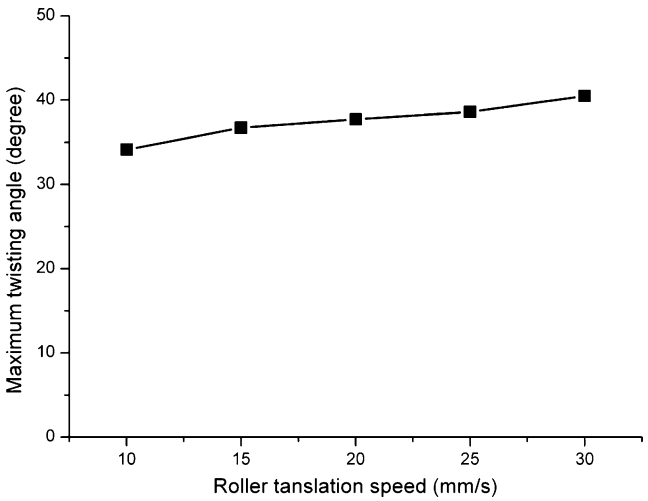

Fig. 17 The influence of roller translation speed on the twisting angle

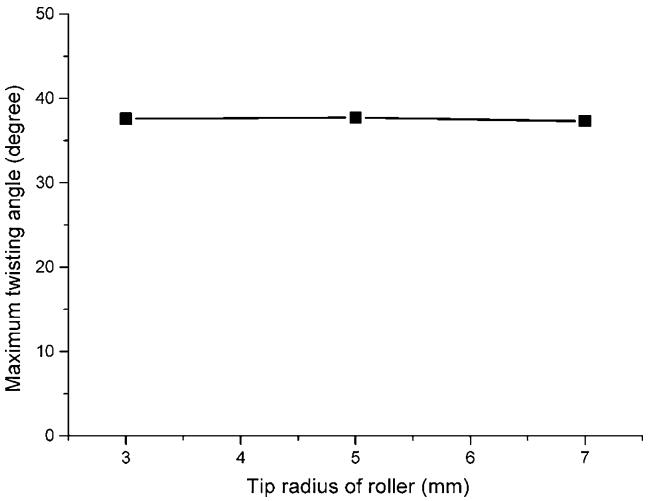

Fig. 20 The influence of roller tip radius on twisting angle

the coefficient of friction increased. Therefore, measuring the twisting angle in an experiment can verify the coefficient of friction in a simulation. Possible methods for showing the twisting angle include printing circular grids [12] and sketching longitudinal lines [20] on the tube surface. However, these marks will disappear after tube spinning at elevated temperature; so currently, methods to measure the twisting angle are still in the developmental stage.

4.3 The influences of roller translation speed

During the neck-spinning process, roller translation speed is an important control parameter. Therefore, various roller translation speeds (10, 15, 20, 25, and 30 mm/s) were used in the simulation. Figure 16 shows the influence of roller translation speed on roundness. The radius deviation increased gradually as the roller translation speed increased; however, ellipticity did not; nevertheless, tendency of ellipticity is rising. Figure 17 shows the influence of roller translation speed on twisting angle. The twisting angle increased slightly as the roller translation speed increased. The conclusion is that the roundness of a tube will decrease as the roller translation speed increases.

4.4 The influences of roller tip radius

The tip radius is an important geometric parameter of a roller during the neck-spinning process. Therefore, various roller tip radiuses (3, 5, and 7 mm) were used in the simulation. Figure 18 shows the dimension of the roller with various tip radiuses. Figure 19 shows the influence of the roller tip radius on roundness. The ellipticity and radius deviation of the tube increased as the tip radius of the roller increased. When the tip radius of the roller was 7 mm, the ellipticity and radius of the tube were significantly larger than those of the other tip radiuses were. Figure 20 shows that there was no significant influence of the roller tip radius on the twisting angle. This suggests that a smaller roller tip radius will produce better tube roundness.

5 Conclusions

In this study, the neck-spinning process of a tube at elevated temperature was analyzed experimentally and numerically. Uniaxial tensile tests were executed at an elevated temperature and various strain rates. The strain rate effect of flow stress was successfully considered in the simulation. The experimental and simulation results of the thickness distribution and outer contour of the spun tube were discussed. During the final stage, the average deviations between the simulation and experiment were 10.65% in thickness and 3.03% in outer contour. The simulation results agreed with those found in the experiment.

Based on the verified FE model for neck-spinning of a tube at elevated temperature, the influences of forming parameters are obtained and conducted as follows:

1. During the neck-spinning process, the twisting angle between the top and bottom of the spun tube increases significantly as the coefficient of friction increases.
2. The roundness of the tube decreases as the roller translation speed increases.
3. During the neck-spinning process, the ellipticity and radius deviation of a spun tube increases as the roller tip radius increases.

Acknowledgments The authors would like to thank the National Science Council of Taiwan, ROC for the grant NSC 98-2622-8-009-016-B2, under which supported the investigation. The authors would also like to thank the National Center for High-Performance Computing and Mosa Industrial Corporation for providing computation and experimental facilities.

References

1. Jianguo Y, Makoto M (2002) An experimental study on paraxial spinning of one tube end. J Mater Process Technol 128:324–329. doi:10.1016/S0924-0136(02)00473-9
2. Jianguo Y, Makoto M (2005) An experimental study on spinning of taper shape on tube end. J Mater Process Technol 166:405–410. doi:10.1016/j.jmatprotec.2004.08.025
3. Roy MJ, Klassen RJ, Wood JT (2009) Evolution of plastic strain during a flow forming process. J Mater Process Technol 209:1018–1025. doi:10.1016/j.jmatprotec.2008.03.030
4. Shan D, Lu Y, Li P, Xu Y (2001) Experimental study on process of cold-power spinning of Ti–15–3 alloy. J Mater Process Technol 115:380–383. doi:10.1016/S0924-0136(01)00827-5
5. Rotarescu MI (1995) A theoretical analysis of tube spinning using balls. J Mater Process Technol 54:224–229. doi:10.1016/0924-0136(94)01772-7
6. Park JW, Kim YH, Bae WB (1997) Analysis of tube-spinning processes by the upper-bound stream-function method. J Mater Process Technol 66:195–203. doi:10.1016/S0924-0136(96)02519-8
7. Molladavoudi HR, Djavanroodi F (2010) Experimental study of thickness reduction effects on mechanical properties and spinning accuracy of aluminum 7075-O, during flow forming. Int J Adv Manuf Technol. doi:10.1007/s00170-010-2782-4
8. Fazeli AR, Ghoreishi M (2011) Statistical analysis of dimensional changes in thermo-mechanical tube-spinning process. Int J Adv Manuf Technol 52:597–607. doi:10.1007/s00170-010-2780-6
9. Hauk S, Vazquez VH, Altan T (2000) Finite element simulation of the flow-splitting-process. J Mater Process Technol 98:70–80. doi:10.1016/S0924-0136(99)00307-6
10. Iguchi T, Yoshitake A, Irie T, Morikawa A (2004) Numerical simulation and development of tube spinning process for exhaust system components of motor vehicles. AIP Conf Proc 712:1077–1082. doi:10.1063/1.1766671

11. Hua FA, Yang YS, Zhang YN, Guo MH, Guo DY, Tong WH, Hu ZQ (2005) Three-dimensional finite element analysis of tube spinning. J Mater Process Technol 168:68–74. doi:10.1016/j.jmatprotec.2004.10.014
12. Xia QX, Xie SW, Huo YL, Ruan F (2008) Numerical simulation and experimental research on the multi-pass neck-spinning of non-axisymmetric offset tube. J Mater Process Technol 206:500–508. doi:10.1016/j.jmatprotec.2007.12.066
13. Parsa MH, Pazooki AMA, Ahmadabadi MN (2009) Flow-forming and flow formability simulation. Int J Adv Manuf Technol 42:463–473. doi:10.1007/s00170-008-1624-0
14. Li Y, Xu Z, Tang Y, Zeng Z (2010) Forming characteristics analysis of the cross-section of axially inner grooved copper tube. Int J Adv Manuf Technol 47:1023–1031. doi:10.1007/s00170-009-2237-y
15. Murata M, Kuboki T, Murai T (2005) Compression spinning of circular magnesium tube using heated roller tool. J Mater Process Technol 162–163:540–545. doi:10.1016/j.jmatprotec.2005.02.199
16. Mori KI, Ishiguro M, Isomura Y (2009) Hot shear spinning of cast aluminium alloy parts. J Mater Process Technol 209:3621–3627. doi:10.1016/j.jmatprotec.2008.08.018
17. Yang H, Huang L, Zhan M (2010) Coupled thermo-mechanical FE simulation of hot splitting spinning process of magnesium alloy AZ31. Comput Mater Sci 47:857–866. doi:10.1016/j.commatsci.2009.11.014
18. Wong CC, Danno A, Tong KK, Yong MS (2008) Cold rotary forming of thin-wall component from flat-disc blank. J Mater Process Technol 208:53–62. doi:10.1016/j.jmatprotec.2007.12.123
19. Mielnik EM (1993) Metalworking science and engineering. McGraw-Hill, New York, p 493
20. Mohebbi MS, Akbarzadeh A (2010) Experimental study and FEM analysis of redundant strains on flow forming of tubes. J Mater Process Technol 210:389–395. doi:10.1016/j.jmatprotec.2009.09.028